Force, Impedance, and Trajectory Learning for Contact Tooling and Haptic Identification

Yanan Li, Gowrishankar Ganesh, Nathanaël Jarrassé, Sami Haddadin, Alin Albu-Schaeffer, Etienne Burdet

Force, Impedance and Trajectory Learning for Contact Tooling and Haptic Identification

Yanan Li*, *Member, IEEE*, Gowrishankar Ganesh*, *Member, IEEE*, Nathanael Jarrassé*, Sami Haddadin, *Member, IEEE*, Alin Albu-Schaeffer, *Member, IEEE*, and Etienne Burdet, *Member, IEEE*

***Abstract*—Humans can skilfully use tools and interact with the environment by adapting their movement trajectory, contact force, and impedance, as was described in [1]. Motivated by the human versatility, and using the algorithm from [1], we develop here a robot controller that concurrently adapts feedforward force, impedance and reference trajectory when interacting with an unknown environment. In particular, the robot's reference trajectory is adapted to limit the interaction force and maintain it at a desired level, while feedforward force and impedance adaptation compensates for the interaction with the environment. An analysis of the interaction dynamics using Lyapunov theory yields the conditions for convergence of the closed-loop interaction mediated by this controller. Simulations exhibit adaptive properties similar to human motor adaptation. The implementation of this controller for typical interaction tasks including drilling, cutting and haptic exploration shows that this controller can outperform conventional controllers in contact tooling.**

I. Introduction

Contact tooling, such as drilling and carving, require dealing with the intrinsic instability resulting from the surface irregularities, unknown material properties, and motor noise. This control problem is exacerbated by the large forces often encountered during these tasks. Furthermore, contact tooling involves deformation or penetration of an object's surface, such that visual feedback is of little help to controllers. All these issues requisite the development of a suitable control strategy for regulating the movement and interaction force during contact tooling tasks.

Various interaction control techniques have been proposed by previous works. These include the *hybrid force-position control* [2], that decouples the force and position control in space, regulating position along the surface of an object and force normal to it. Good performance with this technique thus requires knowledge or good estimation of the surface geometry [3]. For instance, in [3], [4] the surface geometry is estimated from the interaction force and position information. By regulating the relationship between the environment deformation and the force response, *impedance control* [5] can deal with environments that are not precisely known. However, controllers with fixed impedance do not a-priori consider the instability arising from tool use, nor can they adapt to unknown surface conditions [6], [7], [8].

In contrast, humans can carry out unstable tooling tasks with ease, such as carving wooden pieces with knots, using a screwdriver, cutting with a knife, etc. This is arguably due to their capability to automatically compensate for the forces and instability in their environment [9], [10], [11]. We recently developed a computational model of this learning, which enabled us to simulate the characteristics of human motor learning in various stable and unstable dynamic environments [12], [13].

The dynamic properties of this learning controller were analysed in [14], and used to demonstrate its capabilities for robot interaction control. This new robot behaviour can adapt its end-point force and impedance to compensate for environmental disturbances. This controller increases robot force with the signed error relative to a given planned trajectory, increases the impedance when the unsigned error magnitude is large, and decreases impedance when the magnitude is small. While our previous controller in [14] can adapt to various environments, an obstacle on the robot reference trajectory can lead the force to increase and become very large.

How does the human sensorimotor control address this issue? Recent works that examined how humans interact with rigid objects [15], [16] found that the reference trajectory is deformed by the interaction with the object's surface, which limits and regulates the interaction force. We introduced in [1] a model of the concurrent adaptation of impedance, force and trajectory characterising the human adaptive behaviour, and showed in simulation how it could predict human motor adaptation in various conditions. The extended nonlinear adaptive controller implementing this model adapts impedance and force, and guarantees the interaction stability by compensating for the disturbance from the environment, as is analysed in the present paper. The interaction force is continuously estimated and used to adapt the reference trajectory so that the actual interaction force can be maintained at a desired level.

The model of human motor adaptation in [1] can be analysed using Lyapunov theory, and used as a novel iterative learning controller (ILC) for robots. Specifically, we show in the present manuscript how the coupling between

This research was supported by the European Commission grants EU-FP7 VIACTORS (ICT 231554) and CONTEST (ITN 317488), and EU-H2020 COGIMON (644727).

*: The first three authors contributed equally to the work.

Y. Li, G. Ganesh, N. Jarrassé and E. Burdet are or were with the Department of Bioengineering, Imperial College of Science, Technology and Medicine, SW7 2AZ London, UK.

Y. Li is with the Department of Engineering and Informatics, University of Sussex, Brighton, BN1 9RH, UK.

G. Ganesh is with the CNRS-AIST joint robotics lab, Intelligent Systems and Research Institute, Tsukuba, Japan.

N. Jarrassé is with CNRS, ISIR, UPMC Paris VI, France.

S. Haddadin and A. Albu-Schaeffer are or were with the German Aerospace Center, Wessling 82234, Germany.

S. Haddadin is with the Institute of Automatic Control, Leibniz Universitt Hannover, Hannover, Germany.

force/impedance adaptation and trajectory adaptation can be resolved. Simulations are used to study and exhibit the adaptation features. Implementations on DLR's 7-degree-of-freedom light weight robot (LWR) [17], [18] explore its use for representative tasks such as cutting, drilling and haptic exploration similar to polishing, and demonstrate its versatility. Initial results were reported in [19], [20] while extensive results are presented and analysed in this paper. A video illustrating the experiments can be found at https://www.youtube.com/watch?v=UZFL6oTHQBg or on last author's website.

While ICL has been investigated extensively [21], [22], [23], [24], the present paper analyzes for the first time the coupling between impedance and/or force adaptation and trajectory adaptation. This coupling is interesting, since the updated impedance and/or force is used to adapt the reference trajectory and conversely the updated reference trajectory is also used to adapt the impedance/force. Section II and Appendix A extend the algorithm of [14] with trajectory adaptation to yield force control and adaptation of the shape and impedance of the environment. Section III interprets the theoretical results of Section II, Section IV illustrates the controller's functions through simulations, and Section V demonstrates its efficiency in implementations.

TABLE I
NOMENCLATURE

x	actual trajectory vector
q	joint angle vector
M, C, G	inertia, Coriolis and centrifugal, gravitational matrices
u	control input
f	interaction force from the environment
v	control component for compensation of robot's dynamics in free movements
w	control component for adaptation of force, stiffness and damping to interact with a novel environment
x_r	reference trajectory
e	tracking error
x_e	auxiliary trajectory
ε	auxiliary tracking error
Γ	linear control gain for free movements
L	positive-definite gain matrices
F^*, K_S^*, K_D^*, x_0^*	parameters of linear expansion of the environment mechanics: force, stiffness, damping and rest position
F, K_S, K_D	feedforward force, stiffness and damping of controller
Q_F, Q_K, Q_D, Q_r	learning rates for force, stiffness, damping and trajectory
β	decay rate of force, stiffness and damping
F_d	desired interaction force
J_c, J_e, J_r, J	costs of: impedance residual errors, tracking error, contact force error, and overall cost
T	movement trial or period
$\tilde{\bullet}$	$\bullet^* - \bullet$: difference of
$\triangle\bullet$	$\bullet(t+T) - \bullet(t)$: change of a factor during one period

II. ADAPTATION OF FORCE, IMPEDANCE AND PLANNED TRAJECTORY

In the following we derive a general ILC for the interaction of a robot with an environment solely characterized by its stiffness and damping, using Lyapunov theory. The nomenclatures that will be used are summarised in Table I.

A. Controller design

The dynamics of a n-DOF robot in the operational space are given by

$$M(q)\,\ddot{x} + C(q,\dot{q})\,\dot{x} + G(q) = u + f \tag{1}$$

where x is the position of the robot and q the vector of joint angle. u is the control input and f the interaction force applied by the environment. $M(q)$ denotes the inertia matrix, $C(q,\dot{q})\dot{x}$ the Coriolis and centrifugal forces, and $G(q)$ the gravitational force, which can be identified using e.g. nonlinear adaptive control [25].

The control input u is separated in two parts:

$$u = v + w\,. \tag{2}$$

In this equation, v is designed using a feedback linearisation approach to track the *reference trajectory* x_r by compensating for the robot's dynamics, i.e.

$$v = M(q)\,\ddot{x}_e + C(q,\dot{q})\,\dot{x}_e + G(q) - \Gamma\varepsilon \tag{3}$$

where

$$\dot{x}_e = \dot{x}_r - \alpha e\,, \quad e \equiv x - x_r\,, \quad \alpha > 0\,, \tag{4}$$

$\dot{x}_e$ is an auxiliary variable and e is the tracking error. Γ is a symmetric positive-definite matrix having minimal eigenvalue $\lambda_{\min}(\Gamma) \geqslant \lambda_\Gamma > 0$ and ε is the sliding error

$$\varepsilon \equiv \dot{e} + \alpha\, e \tag{5}$$

w, the second part of the control input u, is to adapt impedance and force in order to compensate for the unknown interaction dynamics with the environment, as will be described in this paragraph. *Assuming that the environment can be characterized (locally) by its visco-elasticity*, the interaction force can be expanded as

$$f = F_0^* + K_S^*(x - x_0^*) + K_D^*\dot{x}\,, \tag{6}$$

where $F_0^*(t)$, $K_S^*(t)$ and $K_D^*(t)$ are force, stiffness and damping experienced during interaction with the environment, respectively, $x_0^*(t)$ is the rest position of the environment visco-elasticity. We use Eq.(6) to describe a general environment, which can be either passive with the force component $F_0^* = 0$ or active, such as a human arm or another robot. In this paper, we consider that the environment parameters are unknown but periodic with T:

$$\begin{aligned} F_0^*(t+T) &\equiv F_0^*(t)\,, \quad K_S^*(t+T) \equiv K_S^*(t)\,, \\ K_D^*(t+T) &\equiv K_D^*(t)\,, \quad x_0^*(t+T) \equiv x_0^*(t)\,. \end{aligned} \tag{7}$$

The periodicity of the environment parameters is a realistic assumption for a repeatable interaction task, e.g., the surface exploration presented in the simulation of Section IV. In this example, the properties of the environment surface are the same for every session, so they are periodic along the time axis. In many applications, the environment parameters

are constant thus also periodic. To simplify the analysis, we rewrite the interaction force of Eq.(6) as

$$f \equiv F^* + K_S^* x + K_D^* \dot{x} \tag{8}$$

with $F^* \equiv F_0^* - K_S^* x_0^*$ the feedforward force component of the environment. w in Eq.(2) is then defined as

$$w = -F - K_S x - K_D \dot{x} \tag{9}$$

where F, K_S and K_D are feedforward force, stiffness and damping components in the control input. As explained in next paragraph, the contact stability is ensured through adapting F, K_S, K_D to match the environment's values F^*, K_S^*, K_D^*.

B. Force and impedance adaptation

By substituting the control input u into Eq.(1), the closed-loop system dynamics are described by

$$M(q)\,\dot{\varepsilon} + C(q,\dot{q})\,\varepsilon + \Gamma\varepsilon = \widetilde{F} + \widetilde{K}_S\, x + \widetilde{K}_D\, \dot{x}\,, \tag{10}$$

$$\widetilde{F} \equiv F^* - F\,, \quad \widetilde{K}_S \equiv K_S^* - K_S\,, \quad \widetilde{K}_D \equiv K_D^* - K_D\,.$$

In this equation, we see that the feedforward force F, stiffness K_S and damping K_D ensure contact stability by compensating for the interaction dynamics. Therefore, the objective of force and impedance adaptation is to minimise these residual errors. This can be carried out through minimising the cost function

$$\begin{aligned} J_c(t) \;\equiv\; & \frac{1}{2}\int_{t-T}^{t} \widetilde{F}^T Q_F^{-1} \widetilde{F} + \mathrm{vec}^T(\widetilde{K}_S) Q_S^{-1} \mathrm{vec}(\widetilde{K}_S) \\ & + \mathrm{vec}^T(\widetilde{K}_D) Q_D^{-1} \mathrm{vec}(\widetilde{K}_D)\, d\tau \end{aligned} \tag{11}$$

where Q_F, Q_S and Q_D are symmetric positive-definite matrices, and vec$(\cdot)$ stands for the column vectorization operation. This objective is achieved through the following update laws:

$$\begin{aligned} \Delta F(t) &\equiv F(t) - F(t-T) = Q_F[\varepsilon(t) - \beta(t) F(t)] \\ \Delta K_S(t) &\equiv K_S(t) - K_S(t-T) = Q_S[\varepsilon(t) x(t)^T - \beta(t) K_S(t)] \\ \Delta K_D(t) &\equiv K_D(t) - K_D(t-T) = Q_D[\varepsilon\, \dot{x}(t)^T - \beta(t) K_D(t)] \end{aligned} \tag{12}$$

where F, K_S and K_D are initialised as zero matrices/vectors with proper dimensions when their arguments are within $[0, T)$, and β is a decay factor. Concurrent adaptation of force and impedance in Eq.(12) corresponds to the computational model of human motor adaptation of [12], [13], [14].

Now that we have dealt with the interaction dynamics, trajectory tracking control can be obtained by minimising the cost function

$$J_e(t) \equiv \frac{1}{2}\varepsilon(t)^T M(q)\, \varepsilon(t)\,. \tag{13}$$

Consequently, we use a combined cost function

$$J \equiv J_c + J_e \tag{14}$$

that yields concurrent minimisation of tracking error and residual impedance errors to adapt force and mechanical impedance during movement.

C. Trajectory adaptation

The investigation of adaptation to stiff and compliant environments of [15] has shown that humans tend to apply a constant force on the surface, resulting in a different trajectory adaptation strategy depending on the surface stiffness. To model this observation, *we assume that the trajectory is adapted to maintain a desired contact force F_d with the environment's surface*. In particular, assuming that there exists a desired trajectory x_d yielding F_d, i.e. from Eq.(6)

$$\begin{aligned} F_d &= F_0^* + K_S^*(x_d - x_0^*) + K_D^*\, \dot{x}_d \\ &= F^* + K_S^*\, x_d + K_D^*\, \dot{x}_d \end{aligned} \tag{15}$$

we propose to adapt the reference x_r in order to track x_d. However, x_d is unknown, because the parameters F^*, K_S^* and K_D^* in the interaction force are unknown. Nevertheless, we know that x_d is periodic with T, as F^*, K_S^* and K_D^* are periodic with T and we also set F_d to be periodic with T.

In the following, we develop an update law to learn the desired trajectory x_d. First, we define

$$\xi_d \equiv K_S^*\, x_d + K_D^*\, \dot{x}_d\,, \quad \xi_r \equiv K_S\, x_r + K_D\, \dot{x}_r\,. \tag{16}$$

Then, we develop the following update law

$$\Delta\xi_r(t) \equiv \xi_r(t) - \xi_r(t-T) \equiv L^{-T} Q_r [F_d(t) - F(t) - \xi_r(t)] \tag{17}$$

where Q_r and L are positive-definite constant gain matrices. This update law is developed to minimise the error between the desired force F_d and control force $-w = F + \xi_r$ as detailed in Appendix A. To consider the coupling of adaptation of force and impedance and trajectory adaptation, we modify the adaptation of feedforward force Eq.(12) to

$$\Delta F(t) = Q_F[\varepsilon(t) - \beta(t) F(t) + Q_r^T \Delta\xi_r(t)]\,. \tag{18}$$

Then, we obtain the update law for trajectory adaptation

$$\Delta x_r \equiv x_r(t) - x_r(t-T) \tag{19}$$

by solving

$$\Delta\xi_r = K_S\, \Delta x_r + K_D\, \Delta\dot{x}_r + \Delta K_S\, x_r + \Delta K_D\, \dot{x}_r \tag{20}$$

using $\Delta\xi_r(t)$ from Eq.(17), and $\Delta K_S, \Delta K_D$ from Eq.(12).

With Eqs.(12), (17) and (18) we now have an algorithm able to adapt force, impedance and trajectory in various dynamic environments. This is carried out by minimising the overall cost $J \equiv J_c + J_e + J_r$ where

$$J_r \equiv \frac{1}{2}\int_{t-T}^{t} (\xi_r - \xi_d)^T Q_r^T (\xi_r - \xi_d)\, d\tau\,. \tag{21}$$

The result of this minimisation is summarised in the following theorem:

Theorem 1*: Considering the robot dynamics (1) and the interaction force model (8), the controller (2) with the update laws for stiffness and damping (12), feedforward force (18) and reference trajectory (17) will guarantee that the trajectory error $\Delta\xi_r$ and tracking error ε are bounded and satisfy*

$$\lambda_\Gamma \|\varepsilon\|^2 + \lambda_L \|\Delta\xi_r\|^2 \le \frac{\beta}{2}\left(\|F^*\|^2 + \|vec(K_S^*)\|^2 + \|vec(K_D^*)\|^2\right) \tag{22}$$

for $t \to \infty$, where λ_Γ and λ_L are the minimal eigenvalues of Γ and L, respectively. It follows that $\Delta\xi_r$ and ε can be

made arbitrarily small by choosing sufficiently large λ_Γ and λ_L. Moreover, $\Delta\xi_r$ and ε will converge to zero for $\beta \equiv 0$.

A proof of Theorem 1 is given in Appendix A based on Lyapunov theory and the structure of the novel controller is illustrated in Fig.1.

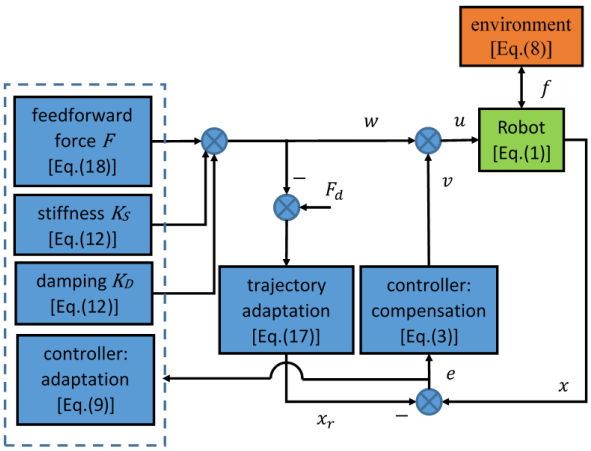

Fig. 1. Block diagram of proposed controller for dynamic interaction with and adaptation to unknown environments. The controller has three components: the dotted block represents the component to learn feedforward force and impedance in order to compensate for the interaction force from the environment; the trajectory adaptation component is to maintain a desired interaction force; and the compensation component compensates for the robot dynamics.

III. Interpretation of Theorem 1

A. Parameters convergence

To simplify the interpretation of Theorem 1, let us loosely state that for $t \to \infty$, $\Delta\xi_r = \varepsilon = 0$ (thus $\dot{\varepsilon} = 0$ if $\lim_{t\to\infty} \dot{\varepsilon}$ exists). With Eq.(17), we obtain $F_d = F + \xi_r$. According to the definitions of w in Eq.(9) and ξ_r in Eq.(16), we have $F + \xi_r = -w$ thus

$$F_d = -w. \tag{23}$$

On the other hand, the right hand side of Eq. (10) is zero. According to the definitions of f in Eq.(8) and w in Eq.(9), we have

$$-w = f. \tag{24}$$

It follows $f = F_d$, which indicates that the desired interaction force F_d is maintained between the robot and the environment. According to the definitions of f and F_d in Eqs.(8) and (15) respectively, we thus have

$$K_S^* x_d + K_D^* \dot{x}_d = K_S^* x + K_D^* \dot{x} \tag{25}$$

which leads to $x \to x_d$ if K_S^* and K_D^* are both positive definite.

However, note that the analysis of Appendix A does not show that F, K_S and K_D converge to the respective values F^*, K_S^* and K_D^* of the environment. This can be seen from Eq.(10): $\widetilde{F} + \widetilde{K}_S\, x + \widetilde{K}_D\, \dot{x} = 0$ does not imply that $\widetilde{F}$, $\widetilde{K}_S$ and $\widetilde{K}_D$ become negligible. In order to achieve the convergence of $\widetilde{F}$, $\widetilde{K}_S$ and $\widetilde{K}_D$ to zero, the signals x and $\dot{x}$ need to satisfy the condition of persistent excitation (PE) as in traditional adaptive control [26]. This will be illustrated in Section IV.

In summary, the proposed controller ensures that the interaction force f follows the desired force F_d and that the reference trajectory x_r follows x_d, the trajectory which yields F_d due to the physical properties of the environment. The controller parameters F, K_S and K_D can track F^*, K_S^* and K_D^* respectively if the signals x and $\dot{x}$ are persistently exciting.

B. Important special cases

If *no force is exerted on the environment*: $f = 0$, the controller component $w = 0$ from Eq.(24). According to the definitions of w in Eq.(9) and ξ_r in Eq.(16), we have $F + \xi_r = -w = 0$. Therefore, if we choose $F_d = 0$, according to the update law Eq.(17), the reference trajectory will not adapt, as expected.

Another important case is when the *feedforward force* $F_0^* = 0$, *damping* $K_D^* = 0$ *and stiffness* $K_S^* \neq 0$, then Eq.(8) yields $x = x_0^*$ if we choose $F_d = 0$ since $f = F_d$. This indicates that the actual position follows the rest position of the environment, i.e. its surface.

If we *neglect the damping* component in the interaction force f of Eq.(8), the trajectory adaptation described by Eqs.(17) and (20) can be simplified to

$$\Delta x_r = L^{-T} Q_r (F_d - F - K_S\, x_r). \tag{26}$$

Correspondingly, the update laws for force and impedance in Eq.(12) need to be modified as

$$\begin{aligned} \Delta F &\equiv Q_F(\varepsilon - \beta F + Q_r^T \Delta x_r)\,, \\ \Delta K_S &\equiv Q_S(\varepsilon\, x^T - \beta K_S + x_r^T Q_r^T \Delta x_r) \end{aligned} \tag{27}$$

in order to obtain results similar to those described in Theorem 1. The interaction dynamics analysis, similar to the case with damping, is detailed in Appendix B.

C. Implicit and explicit force sensing

In contrast to traditional methods for surface following where the force feedback is used to regulate the interaction force e.g. [27], force sensing is not required in the above framework. In particular, force and impedance adaptation (Eqs.(12) and (18)) is used to compensate for the interaction force from the environment. During this process, the unknown actual interaction force is estimated when the tracking error ε goes to zero, i.e., Eq.(24). Using this estimated interaction force, a desired force in Eq.(15) can then be rendered by adaptation of the reference trajectory x_r (Eqs.(17) and (20)).

If the robot system is equipped with a force sensor, force feedback can replace the force and impedance adaptation. In this way, trajectory adaptation will not depend on the force estimation process and can in principle happen faster. However, the potential advantages of a force sensor depend on the quality of its signal, its cost and the difficulty of its installation and use.

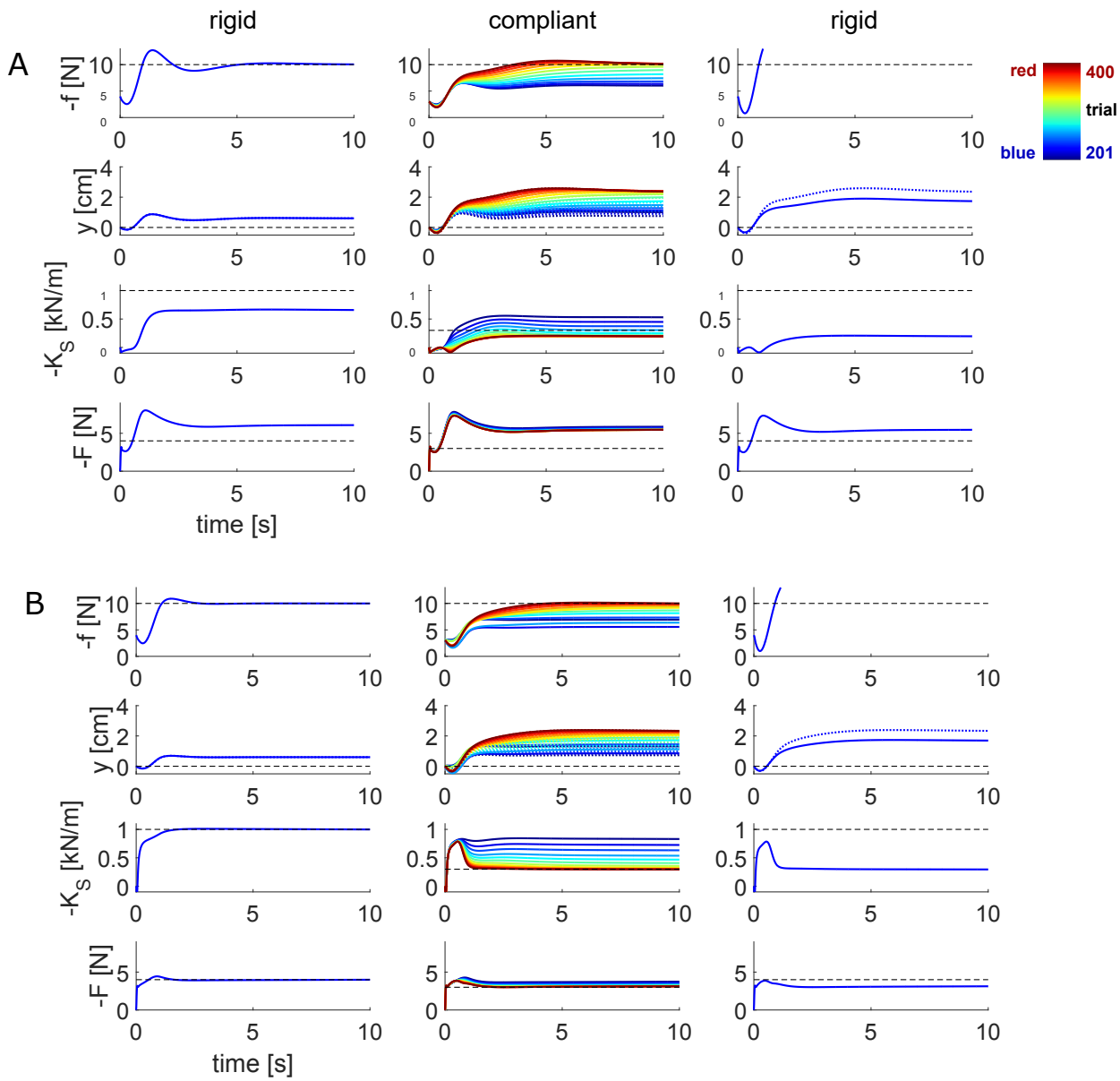

Fig. 2. Concurrent adaption of force, impedance and trajectory without noise (A) and with noise satisfying persistent excitation (B). From top to bottom: interaction force, actual trajectory (solid) and updated reference trajectory (dotted), updated stiffness, and updated feedforward force. From left to right: after learning in a rigid environment, in a compliant environment (plotted from blue to red in every 16 trials), and exposition to a rigid environment after learning in the compliant environment.

IV. Simulations

We will now illustrate how the learning controller of previous section functions, by simulating the human motor adaptation in a representative interaction task [16]. This study observed the adaptation of force and trajectory in humans during contact with a rigid or compliant environment. Similarly, we simulated the adaptation of the reference trajectory occurring when one is required to push against environments of various stiffnesses. In this simulation, the desired force in forward direction is specified as

$$F_d = \begin{cases} -5[1-\cos(\pi t)]N, & 0 \le t \le 1s; \\ -10N, & \text{otherwise.} \end{cases} \tag{28}$$

The interaction force of Eq.(8) is computed as

$$f = F^* + K_S^* \, y \tag{29}$$

corresponding to the rest position 0. The rigid environment is characterised by $F^* = -4N$ and $K_S^* = -1000N/m$ and the compliant environment by $F^* = -3N$ and $K_S^* = -300N/m$. The environment is rigid for the first 200 trials $j = 1 \ldots 200$ and compliant for another 200 trials $j = 201 \ldots 400$. The control and learning parameters used for simulation are $\alpha = 10, \Gamma = 200, \beta = 0, Q_S = 6 \times 10^4, Q_F = 3.6, Q_r = 0.02$.

Simulation results are shown in Fig.2A. The left column/panels exhibit that the desired force is achieved in the case of a rigid environment. The middle panels illustrate that when the environment suddenly becomes compliant, the desired force

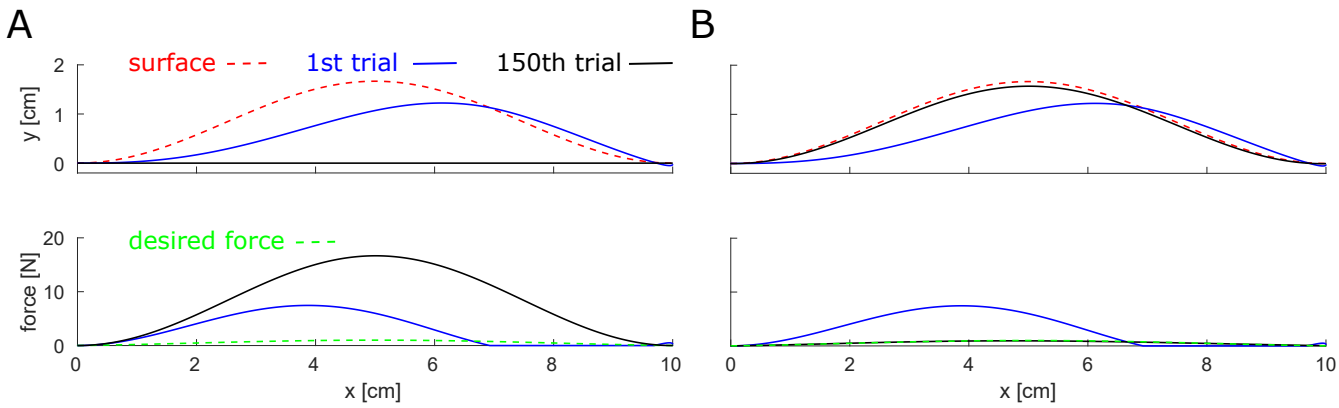

Fig. 3. Simulation of haptic exploration of a surface of unknown shape and mechanical properties along x-axis with the controller of [14] (A) and with the new controller (B). The top panels show the robot's trajectory and the bottom panels the contact force. The new controller avoids large interaction force and enables to regulate the force, while identifying the interaction surface geometry.

cannot be reached because of the trajectory control component. However, the trajectory iteratively moves forward and the interaction force increases. After learning, the reference trajectory has adapted to penetrate the environment surface and the desired interaction force is achieved again. Note that while the same desired force is achieved in the rigid environment, the reference trajectory changes with the different environments. The right panels illustrate the "after-effects" of the learning: when the environment becomes rigid again, the interaction force surpasses the desired force.

These results correspond to the behaviour observed in human experiments [16]. Note the adaptation of force, impedance and trajectory involved in the evolution: the reference trajectory adapts to achieve the desired force, while feedforward force and impedance adapt to track the updated reference trajectory. However, in Fig.2A the updated feedforward force and impedance do not converge to the values of the environment. This is due to the redundancy between the feedforward force and impedance as explained in Section III-A. While the combination of the feedforward force and impedance guarantees compensation for the interaction dynamics, it is not set to identify each component's contribution.

The identification of the environment's parameters can be addressed by introducing a *persistent excitation* (PE) signal yielding sufficiently rich information of the system. We illustrate this by adding a random binary excitation to the system as exhibited in Fig. 2B. It can be seen that the identified interaction force and position values are similar to those in Fig.2A, but in this case the updated feedforward force and impedance converge to the environment's values. The results in Figs.2A and 2B also illustrate the meaning of redundancy between the feedforward force and impedance, as different values of feedforward force and impedance lead to the same interaction force and position. In practice, noise leading to the environment identification could stem from a rough surface along which the robot is moving (see Fig.2B), while sliding on a smooth surface would lead to results similar to that in Fig.2A.

These results, together with the results of [1], show that the model of Section II predicts the adaptation of force, impedance and trajectory observed when humans interact with various stable, unstable, stiff and compliant environments [28], [9], [29], [13], [15], [16].

To illustrate the difference of the new controller relative to adaptive controller of [14], Fig.3 presents a simulation of polishing along (the x-axis of) a curved surface with both of these controllers. As shown in Fig.3A, as the controller of [14] tries to track the original reference trajectory (which is set as a straight line along the x-axis), this leads to a large contact force of around 20N, which is undesirable. In contrast, Fig.3B shows that with the new controller the robot's trajectory comes close to the surface with learning (see "150th trial"), by tracking the updated reference trajectory while the contact force tends to the desired force of about 1N. Therefore, the new adaptive controller is extending the controller of [14]. It is able to successfully perform tasks requiring contact with rigid surfaces of unknown shape, and to identify the geometry and impedance properties of the surface it is interacting with.

V. Robotic Validation

The proposed controller was implemented on the DLR lightweight robot shown in Fig.4 [17], [18] and tested in various experiments. Four tasks were carried out: adaptation to a rigid surface, cutting, drilling and haptic exploration, which are described in this section.

A. Adaptive interaction with a rigid surface

To illustrate the trajectory adaptation to a rigid environment, one axis of the robot was programmed to repeat a movements of 0.7 radian amplitude following a smooth fifth order polynomial reference, with zero start and end velocity and acceleration as shown in Fig.5. After the robot converged on the reference trajectory (dashed blue trace), it was presented with a virtual obstacle in velocity space (blue trace) that prevented it from following the reference. This obstacle was generated by disconnecting the proposed controller output to the motor, and instead moving the robot along the obstacle using a high gain PD controller while the proposed controller was still active in the background. This simulated a situation

Fig. 4. Setup of experiments described in Section V with the DLR lightweight robot (LWR), the Dremel driller attached to the robot end-effector in the zoomed end-effector and the scalpel in the main panel.

where the controller was unable to generate sufficient motor output to overcome the obstacle.

When the obstacle was suddenly removed in the fifth adaptation trial, the robot movement was found to mirror the obstacle (red trace), as the robot initially tried to increase the torque to counter the obstacle. The obstacle was then re-introduced from the sixth trial onwards. When the obstacle was removed again in the 25th trial, the actual trajectory (black trace) and reference trajectory (dashed black trace) can be clearly seen to have adapted to the shape of the obstacle. The robot movement no longer mirrored the obstacle, i.e. it has learnt not to apply a too large force in order to counter the obstacle, but instead has adapted its reference trajectory. The actual trajectory (black trace) can be seen to lie to the right of the plan (dashed black trace), indicating that the robot still did apply some contact force onto the obstacle after 25 trials. This behaviour is similar to the adaptation observed in humans [15] as was analysed in [1].

B. Cutting experiment

Several experiments were then carried out to test adaptation of impedance and force during the interaction with unknown environments. In this purpose, a cutter or a drill was mounted on the LWR as shown in Fig.4. Different from above simulation and the first experiment, in the next experiments iteration was in time rather than by repeating a trajectory. In this case the LWR moved at low speed so that adaptation could catch the environment characteristics along the trajectory. The controller was programmed to tune the adaptation gains differently along each axis of the end-effector frame $\{e_x, e_y, e_z\}$. A fixed high stiffness ($2000N/m$) was maintained at the robot end effector in the $\{y \equiv 0\}$ plane while the adaptive controller was used in the x and z directions. Stiffness saturation was set at $2000N/m$ in all directions during the experiments. The same set of adaptation gains of $\beta = 0.01$, $Q_F = 5$, $Q_S = 120$, $Q_r = 0.01$ was used during all the experiments in order to test the versatility of the adaptive controller in dealing with different tasks and environments without any manual tuning of the learning parameters. Q_r was set as zero in the cutting and drilling experiments.

We performed two cutting experiments using a scalpel that was fixed on the LWR end effector using a customized tool holder. The scalpel blade was maintained at a $65°$ angle to the surface. We used a heterogeneous test object in the first experiment that was made of a $2mm$ balsa wood layer covered by a $2mm$ layer of materials with different mechanical properties: balsa wood, plastic honeycomb panel and brown corrugated cardboard. As can be seen in Fig.6B, the stiffness and feedforward force were automatically adapted during the task to the specific material: stiffness increased due to the vibrations generated during the crossing of the carton and honeycomb sections and decreased during the crossing of the balsa wood section. On the other hand, the feedforward force increased during the crossing of the balsa wood section, because the wood is dense and generates a constant resistance to cutting.

The second cutting experiment was performed on a $3cm$ thick expanded styrofoam board (made of $4mm$ polystyrene balls agglomerated together, but with a smooth surface). The top surface of the board was painted in black to illustrate the damage done to the surface by the scalpel. Due to the material properties of styrofoam, it tends to stick to the blade and tear when the depth is too large for a given speed. We first determined a constant "depth/velocity" pair for our blade that leads to material tear (due to stick-slip) during cutting. Cutting was then carried out with this "depth/velocity" pair, first using a fixed high impedance ($1500N/m$) then with the proposed adaptive controller starting from the same $1500N/m$ stiffness value. As it can be seen in Fig.6C, our adaptive controller avoided the tearing phenomenon generated by the specific set of parameters (e.g., blade angle, velocity and depth) though lowering the robot stiffness.

C. Drilling

We then compared drilling of a heterogeneous material using a fixed impedance ($1500N/m$), and with adaptation using the proposed controller. Drilling was tested using a Dremel hand driller attached to the end-effector (through the force/torque sensor) at approximately $18cm$ from the end-effector main axis. The force/torque sensor was used for the purpose of recording but not used in the proposed controller. The $3.2mm$ diameter drill had to penetrate an heterogeneous block of material made of balsa wood layers (easy to drill) and some dense carton layers (requiring larger forces for drilling). As can be seen in Fig.7, our controller was able to perform the task with results similar to the rigid impedance controller. However, at certain drilling speeds, the rigid impedance controller exhibited a "resonance" phenomenon (see Fig.7B) that generated large vibrations in the horizontal plane (whose amplitude was proportional to the penetration of the drill bit), and consequently poorer quality of the drilled hole (larger variations in the diameter of the hole, as seen in the bottom of Fig.7C). The proposed controller attenuated these vibrations, resulting in a hole with a diameter closer to the real drill bit diameter.

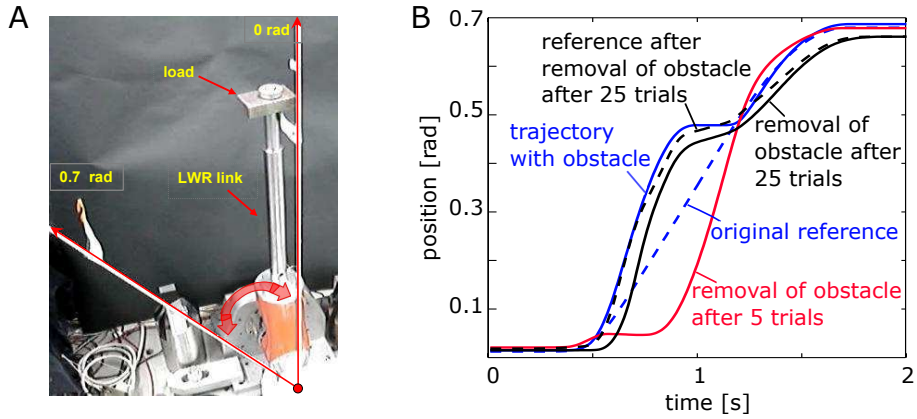

Fig. 5. Adaptation to a rigid surface. A: 1-DOF robot; B: actual and reference trajectories.

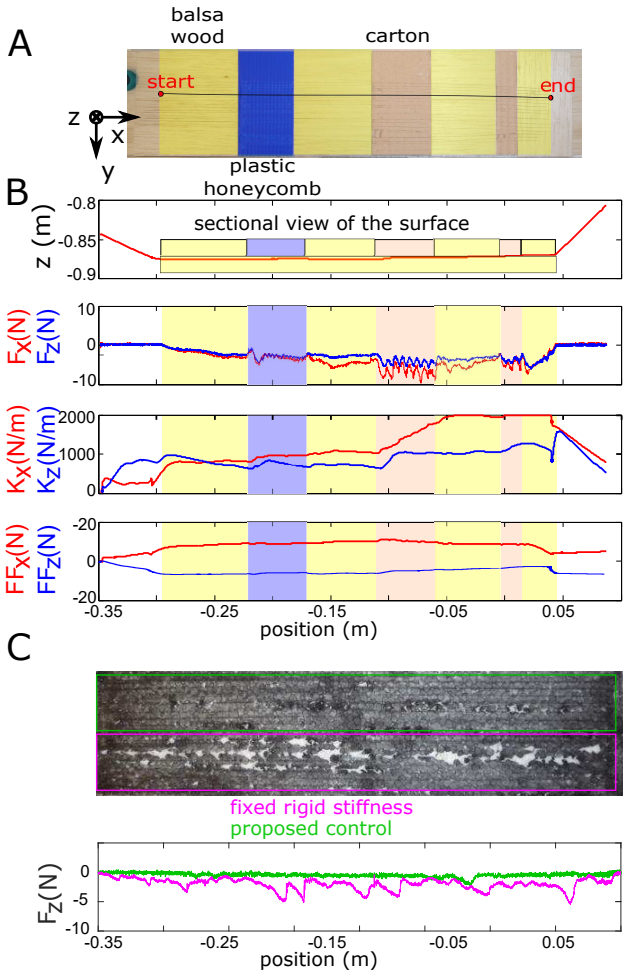

Fig. 6. Cutting through different materials. A: View of the surface assembled with different materials (balsa wood, cardboard and honeycomb plastic). B: From top to bottom: blade trajectory across the section of the surface in the vertical plane; variations of the forces F_x and F_z along x and z directions, recorded by the 6-DOF force/torque sensor mounted between the robot and the scalpel; stiffness (K_x and K_z) and feedforward force (FF_x and FF_z) adaptation during the cutting task. C: Visual results of cutting expanded styrofoam with/out biomimetic adaptation and associated force profile (along the cutting direction x).

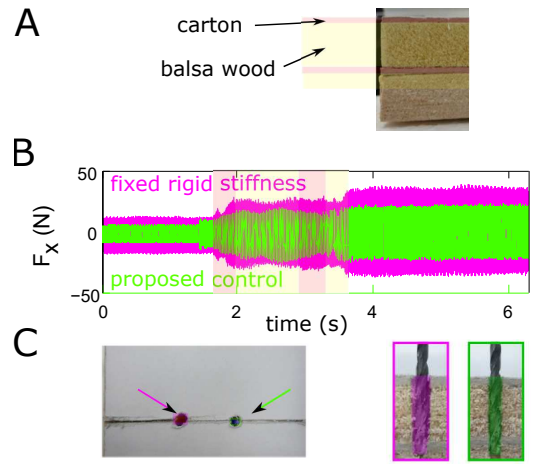

Fig. 7. Drilling heterogeneous material. A: Section of the block. B: Comparison of vibrations level in the horizontal plane transmitted to the robot structure (read on the force sensor) when using a driller speed generating "resonance", without (red) and with (green) stiffness adaptation. C: Adapting impedance reduced the hole carried out by the drill.

D. Haptic identification

To test concurrent adaptation of force, impedance and trajectory, we implemented a haptic exploration experiment. The robot was required to traverse various surface profiles on a test surface while maintaining a constant contact force, a task that is similar to the polishing of an unknown surface. However, we designed the task to test the ability of the new controller to "skim" a surface with minimum force. We purposely used a very low desired interaction force level of 0.05N and a soft foam surface so as to be able to visually check whether the robot would push and deform this surface (see the video in https://www.youtube.com/watch?v=UZFL6oTHQBg).

The test surface was developed on a wooden plank sized $85 \times 95cm$. Various profiles, including convex bumps, concave troughs and cylindrical obstacles were created on this surface by fixing metal and plastic objects (Fig.8A). A $3cm$ thick layer of packing foam was then overlaid on the surface. The test surface included a high friction pad created using twisted nylon ropes and a hole in the surface. The test surface was placed on a table under the robot which was equipped with

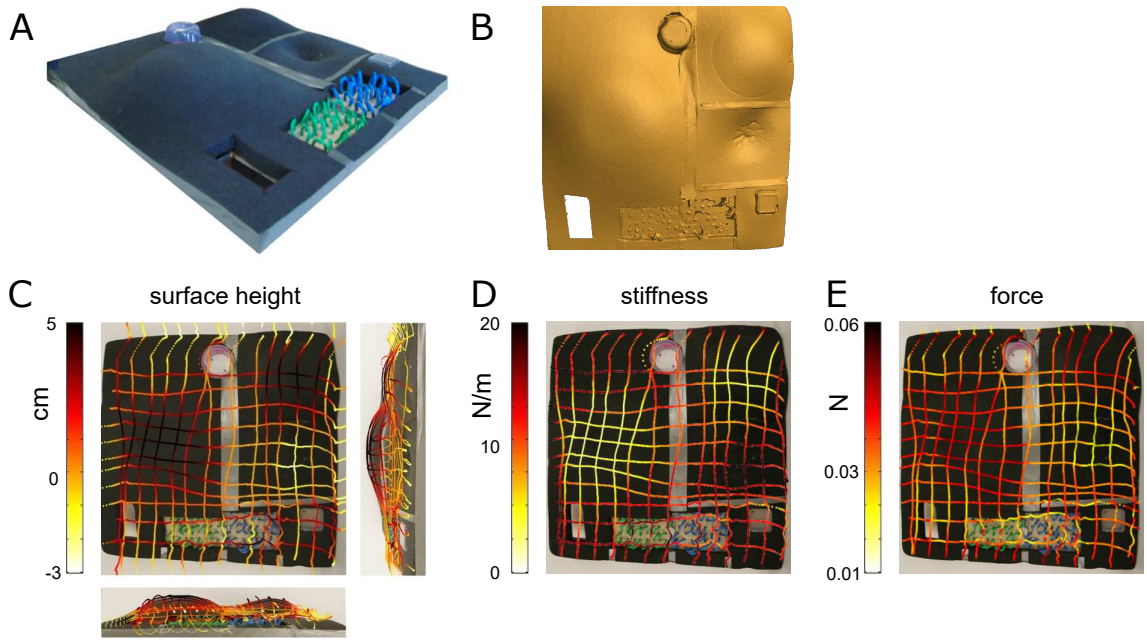

Fig. 8. Haptic exploration of a surface with unknown geometry and mechanics. From left to right: A: Photo of the test surface that was used for the pilot experiment. B: 3D scan of the test surface. C: Volume identified by the robot while scanning the surface along the line superimposed on top and two lateral views. D: End point stiffness during exploration. E: Nearly constant interaction force of about $0.05N$ maintained on the surface.

a $12cm$ long aluminium finger at the end-effector. The robot reference was set to scan the plane of the table over a range of $120cm$ and with a constant speed of $0.1m/s$ (except for the accelerations and de-accelerations in the movement limits). The reference was set in the task space and the trajectory was developed using the interpolator of the manipulator.

Fig.8B shows the surface traced by the robot. Fig.8C shows the tool-tip coordinates of the robot in the x-y plane of the table with the colour gradient representing the z-coordinate (height above the table). Fig.8D plots the endpoint stiffness of the robot as it performed the surface exploration while Fig.8E shows the contact force along the vertical z-axis as measured from the end-point force/torque sensor (not used for control). We conducted an analysis of the force sensor inside the surface boundaries which exhibits a force of 0.0338N in average with a standard deviation of 0.0088N. To show that this is not an offset on the force sensor, or noise, we compared this value to the one from outside the surface in the same experiment. The value from outside the surface (when there is no contact) is 0.0151N in average with a standard deviation of 0.0109N, which is statistically smaller than the one inside the surface boundaries ($p < 0.001$). Stiffness is maintained at a low value throughout the exploration and increases only in the edges of the surface and in the region with irregularities. The stiffness change thus indicates the texture properties of the surface.

VI. Discussion

Many tasks with end-effector held tools are inherently unstable, require large contact forces and are subject to disturbances due to the irregularities on the tooled surface. While robots have been conceived to address these challenges in specific and well defined situations, humans routinely use tools in different tasks such as drilling, cutting and polishing, adapting to various environments, despite large sensorimotor noise. In fact, human intelligence has been characterised by the skilful use of tools [30], and specific neural structures could be identified in humans [31] that correspond to force and impedance adaptations. While we do not pretend to match such manipulation intelligence, the controller analysed in this paper exhibited a versatile interaction behaviour, and was also shown to model human interaction properties in typical situations [1].

Our controller for contact tooling and haptic identification automatically adapts feedforward force, mechanical impedance and trajectory to the environment dynamics in order to minimise trajectory error and effort while applying a desired force. It compensates for the interaction force and instability to track the planned reference trajectory. During this process, the controller is able to estimate the interaction force with the unknown environment through adaptation of feedforward force and impedance. It extends the functionality of the controller introduced in [14], by automatically adapting its reference trajectory to comply with rigid environments, and to maintain a desired interaction force.

The proposed controller, developed based on the assumption of a linearised interaction force (Eq.(6)), can interact with a rigid environment or a compliant force field, or with humans. It can be used to automatically tune physical assistance in e.g. a rehabilitation robot [32]. It does not require a force sensor as the force is estimated by the algorithm. Using a force sensor will however speed up the adaptation of feedforward force, stiffness and trajectory, although this may depend on the quality of the force signal and on its noise.

The stability and convergence of this novel nonlinear adaptive controller have been rigorously analysed using Lyapunov theory. An implementation on the DLR 7-DOF LWR demonstrated its effectiveness and versatility in representative inter-

action tasks including cutting, drilling and haptic exploration. With this controller the robot constantly adapts its behaviour to the environment, rather than rigidly trying to go through. Feedforward force adaptation is essential for tasks like cutting, where the material irregularities continuously modify the required cutting force. Impedance adaptation helps counter these variations while maintaining minimum stiffness of the cutting tool. Trajectory adaptation enables maintenance of contact force during tasks like polishing and prevents the robot from applying very high forces in the presence of unforeseen obstacles.

Experimental results demonstrated superior performance of the novel adaptive controller relative to a fixed impedance controller: smoother interaction, reduced control effort and automatic adaptation (avoiding tedious trial-and-error and fine tuning). Moreover, the properties of the unknown environment could be identified through adaptation during slow interaction movements yielding haptic exploration. As in any tooling task, our algorithm does require some basic parameter definition for each tooling operation such as cutting speed and depth of cut prescribed by tool manufacturer for a given tool-surface combination. However, it does not require any information or model of the surface irregularities, material and shape of the tooled surface.

The proposed controller can be applied to interact with environments that can be described by Eq.(6), characterised by periodic or constant parameters. If the environment parameters keep changing and the periodicity condition is not satisfied, e.g. when interacting with a human arm, the controller can still successfully adapt as long as the environment parameter changes are *slow*, but may fail otherwise. Larger controller learning rates (Q_F, Q_K, Q_D, Q_r) may enable it to adapt to fast changing environments, although too large learning rates may reduce the system robustness. On the other hand, improper choice of initial controller parameters may lead to task failure. For instance, during a surface polishing task, a controller with high initial stiffness can make the robot get stuck in rough stiff surface. The interesting meta learning issue of choosing the appropriate learning rates and initial parameters need to be investigated in further studies.

Appendix

A. Proof of Theorem 1

A Lyapunov-like analysis of the closed-loop learning control is carried out here in four steps. The first three steps consider the difference between two consecutive periods of the Lyapunov function candidates J_r (error of contact force), J_c (residual impedance errors) and J_e (tracking error), respectively. Step 4 then uses the results of the first three steps to examine the difference between two consecutive periods of the overall cost $J \equiv J_r + J_c + J_e$.

Step 1: Contact force error

Considering the definition of J_r in Eq. (21), we have

$$\begin{aligned}
&\Delta J_r(t) \equiv J_r(t) - J_r(t-T) \\
=\ & \frac{1}{2}\int_{t-T}^{t} [\xi_r(\tau) - \xi_d(\tau)]^T Q_r^T [\xi_r(\tau) - \xi_d(\tau)]\, d\tau \\
& -\frac{1}{2}\int_{t-T}^{t} [\xi_r(\tau) - \xi_d(\tau)]^T Q_r^T [\xi_r(\tau-T) - \xi_d(\tau-T)]\, d\tau \\
& +\frac{1}{2}\int_{t-T}^{t} [\xi_r(\tau) - \xi_d(\tau)]^T Q_r^T [\xi_r(\tau-T) - \xi_d(\tau-T)]\, d\tau \\
& -\frac{1}{2}\int_{t-T}^{t} [\xi_r(\tau-T) - \xi_d(\tau-T)]^T Q_r^T \times \\
& [\xi_r(\tau-T) - \xi_d(\tau-T)]\, d\tau \\
=\ & \frac{1}{2}\int_{t-T}^{t} [\xi_r(\tau) - \xi_d(\tau)]^T Q_r^T \Delta\xi_r(\tau)\, d\tau \\
& +\frac{1}{2}\int_{t-T}^{t} [\xi_r(\tau-T) - \xi_d(\tau-T)]^T Q_r^T \Delta\xi_r(\tau)\, d\tau \\
=\ & \int_{t-T}^{t} [\xi_r - \xi_d - \frac{1}{2}\Delta\xi_r]^T Q_r^T \Delta\xi_r\, d\tau \quad (\text{as } \xi_d(t) = \xi_d(t-T)) \\
\leqslant\ & \int_{t-T}^{t} [Q_r(\xi_r(\tau) - \xi_d(\tau))]^T \Delta\xi_r(\tau)\, d\tau\,. \qquad (30)
\end{aligned}$$

According to Eqs.(15) to (17), we rewrite this inequality as

$$\begin{aligned}
\Delta J_r &\leqslant \int_{t-T}^{t} [Q_r(\xi_r - F_d + F + \widetilde{F})]^T \Delta\xi_r\, d\tau \\
&= \int_{t-T}^{t} (-L^T\Delta\xi_r + Q_r\widetilde{F})^T \Delta\xi_r\, d\tau. \qquad (31)
\end{aligned}$$

Step 2: Residual impedance error

Consider the difference between J_c of two consecutive periods

$$\begin{aligned}
\Delta J_c &\equiv J_c - J_c(t-T) \qquad (32) \\
&= \frac{1}{2}\int_{t-T}^{t} [(\widetilde{F}^T Q_F^{-1}\widetilde{F} - \widetilde{F}^T(\tau-T) Q_F^{-1}\widetilde{F}(\tau-T)) \\
&\quad +\mathrm{tr}(\widetilde{K}_S^T Q_S^{-1}\widetilde{K}_S - \widetilde{K}_S^T(\tau-T) Q_S^{-1}\widetilde{K}_S(\tau-T) \\
&\quad +(\widetilde{K}_D^T Q_D^{-1}\widetilde{K}_D - \widetilde{K}_D^T(\tau-T) Q_D^{-1}\widetilde{K}_D(\tau-T))]\, d\tau
\end{aligned}$$

where $\mathrm{tr}(\cdot)$ stands for the trace of a matrix. We compute

$$\begin{aligned}
& \widetilde{F}^T(\tau) Q_F^{-1}\widetilde{F}(\tau) - \widetilde{F}^T(\tau-T) Q_F^{-1}\widetilde{F}(\tau-T) \\
=\ & [\widetilde{F}^T(\tau) Q_F^{-1}\widetilde{F}(\tau) - \widetilde{F}^T(\tau) Q_F^{-1}\widetilde{F}(\tau-T)] \\
& +[\widetilde{F}^T(\tau) Q_F^{-1}\widetilde{F}(\tau-T) - \widetilde{F}^T(\tau-T) Q_F^{-1}\widetilde{F}(\tau-T)] \\
=\ & -\widetilde{F}^T(\tau) Q_F^{-1}\Delta F(\tau) - \widetilde{F}^T(\tau-T) Q_F^{-1}\Delta F(\tau) \\
=\ & -(2\widetilde{F}^T(\tau) + \Delta F(\tau)) Q_F^{-1}\Delta F(\tau) \\
\leqslant\ & -2\widetilde{F}^T(\tau) Q_F^{-1}\Delta F(\tau) \\
=\ & -2\widetilde{F}^T(\tau)[\varepsilon(\tau) - \beta(\tau)F(\tau) + Q_r^T\Delta\xi_r(\tau)]\,. \qquad (33)
\end{aligned}$$

Similarly we have

$$\begin{aligned}
& \mathrm{tr}[\widetilde{K}_S^T(\tau) Q_S^{-1}\widetilde{K}_S(\tau) - \widetilde{K}_S^T(\tau)(\tau-T) Q_S^{-1}\widetilde{K}_S(\tau-T)] \\
& \leqslant -2\mathrm{tr}\{\widetilde{K}_S^T(\tau)[\varepsilon(\tau)x^T(\tau) - \beta(\tau)K_S(\tau)]\} \\
& \mathrm{tr}[\widetilde{K}_D^T(\tau) Q_d^{-1}\widetilde{K}_D(\tau) - \widetilde{K}_D^T(\tau-T) Q_D^{-1}\widetilde{K}_D(\tau-T)] \\
& \leqslant -2\mathrm{tr}[\widetilde{K}_D^T(\tau)(\varepsilon(\tau)\dot{x}^T(\tau) - \beta(\tau)K_D(\tau))]\,. \qquad (34)
\end{aligned}$$

Substituting Ineqs. (33) and (34) into Eq.(32) and considering Ineq. (31), we obtain

$$\Delta J_r + \Delta J_c \leqslant \int_{t-T}^{t} -\Delta\xi_r^T L \Delta\xi_r - \widetilde{F}^T(\varepsilon - \beta F) \qquad (35)$$
$$- \text{tr}[\widetilde{K}_S^T(\varepsilon x^T - \beta K_S)] - \text{tr}[\widetilde{K}_D^T(\varepsilon \dot{x}^T - \beta K_D)]\, d\tau\,.$$

Step 3: Tracking error
The rest of the derivations deals with the residual in above inequality, which is similar to that in [14]. For completeness, we outline this in the following. In particular, we consider the time derivative of J_e

$$\dot{J}_e = \varepsilon^T M \dot{\varepsilon} + \frac{1}{2}\varepsilon^T \dot{M} \varepsilon = \varepsilon^T M \dot{\varepsilon} + \varepsilon^T C \varepsilon \qquad (36)$$

as [33]

$$z^T \dot{M} z \equiv 2 z^T C z \quad \forall z\,. \qquad (37)$$

Considering the closed-loop dynamics Eq.(10), above equation can be written as

$$\dot{J}_e(t) \equiv \varepsilon^T(\widetilde{F}^T + \widetilde{K}_S^T\, x + \widetilde{K}_D^T\, \dot{x} - \Gamma\varepsilon)\,. \qquad (38)$$

Integrating $\dot{J}_e$ from $t-T$ to t and considering Ineq. (35), we obtain

$$\Delta J_e = \int_{t-T}^{t} -\varepsilon^T \Gamma \varepsilon + \widetilde{F}^T \varepsilon + \text{tr}(\widetilde{K}_S^T \varepsilon x^T) + \text{tr}(\widetilde{K}_D^T \varepsilon \dot{x}^T)\, d\tau\,. \quad (39)$$

Step 4: Overall cost J
Considering Ineq.(35) and Eq.(39), we can now calculate

$$\begin{aligned}
\Delta J &= \Delta J_c + \Delta J_r + \Delta J_e \\
&\leqslant \int_{t-T}^{t} -\varepsilon^T \Gamma \varepsilon - \Delta\xi_r^T L \Delta\xi_r \\
&\qquad + \beta[\widetilde{F}^T F + \text{tr}(\widetilde{K}_S^T K_S + \widetilde{K}_D^T K_D)]\, d\tau \\
&= \int_{t-T}^{t} -\varepsilon^T \Gamma \varepsilon - \Delta\xi_r^T L \Delta\xi_r - \beta[\widetilde{F}^T \widetilde{F} + \text{tr}(\widetilde{K}_S^T \widetilde{K}_S + \widetilde{K}_D^T \widetilde{K}_D)] \\
&\qquad + \beta[\widetilde{F}^T F^* + \text{tr}(\widetilde{K}_S^T K_S^* + \widetilde{K}_D^T K_D^*)]\, d\tau\,. \qquad (40)
\end{aligned}$$

According to (40), a sufficient condition for $\Delta J \leqslant 0$ is

$$\begin{aligned}
&\lambda_\Gamma \|\varepsilon\|^2 + \lambda_L \|\Delta\xi_r\|^2 + \beta(\|\widetilde{F}\|^2 + \|\text{vec}(\widetilde{K}_S)\|^2 \\
&+ \|\text{vec}(\widetilde{K}_D)\|^2) - \beta(\|\widetilde{F}\|\|F^*\| + \|\text{vec}(\widetilde{K}_S)\|\|\text{vec}(K_S^*)\| \\
&+ \|\text{vec}(\widetilde{K}_D)\|\|\text{vec}(K_D^*)\|) \geq 0 \qquad (41)
\end{aligned}$$

Therefore, the following inequality is satisfied:

$$\begin{aligned}
&\lambda_\Gamma \|\varepsilon\|^2 + \lambda_L \|\Delta\xi_r\|^2 + \frac{\beta}{2}(\|\widetilde{F}\|^2 + \|\text{vec}(\widetilde{K}_S)\|^2 + \|\text{vec}(\widetilde{K}_D)\|^2) \\
&\leq \frac{\beta}{2}(\|F^*\|^2 + \|\text{vec}(K_S^*)\|^2 + \|\text{vec}(K_D^*)\|^2) \qquad (42)
\end{aligned}$$

The above inequality can be proved by contradiction: assuming the above inequality is invalid yields $\Delta J < 0$ and thus J decreases iteratively. This indicates that $\|\varepsilon\|$, $\|\Delta\xi_r\|$, $\|\widetilde{F}\|$, $\|\text{vec}(\widetilde{K}_S)\|$ or $\|\text{vec}(\widetilde{K}_D)\|$ (and thus the left hand side of the above inequality) become even smaller, which contradicts the hypothesis.

From the above inequality, we obtain Ineq.(22), which indicates that $\Delta\xi_r$ and ε can be made arbitrarily small by choosing sufficiently large λ_Γ and λ_L. Moreover, if we select $\beta \equiv 0$, $\Delta\xi_r$ and ε will converge to zero.

B. Stability analysis when neglecting damping

Consider the cost function

$$J_r' \equiv \frac{1}{2}\int_{t-T}^{t} (x_r - x_d)^T K_S^{*T} Q_r^T (x_r - x_d)\, d\tau\,. \qquad (43)$$

Following similar procedures to Ineqs. (30), (31), we obtain

$$\Delta J_r' \leqslant \int_{t-T}^{t} [-L^T \Delta x_r + Q_r(\widetilde{F} + \widetilde{K}_S x_r)]^T \Delta x_r\, d\tau\,. \quad (44)$$

Considering further the cost function

$$J_c' \equiv \frac{1}{2}\int_{t-T}^{t} \widetilde{F}^T Q_F^{-1} \widetilde{F} + \text{vec}^T(\widetilde{K}_S) Q_S^{-1} \text{vec}(\widetilde{K}_S)\, d\tau \quad (45)$$

and following similar procedures from Ineqs.(32) to (35), we obtain

$$\begin{aligned}
\Delta J_r' + \Delta J_c' \quad \leqslant \quad & \int_{t-T}^{t} -\Delta x_r^T L \Delta x_r - \widetilde{F}^T(\varepsilon - \beta F) \\
& - \text{tr}[\widetilde{K}_S^T(\varepsilon\, x^T - \beta K_S)]\, d\tau\,. \qquad (46)
\end{aligned}$$

The rest is similar to the case with damping and thus omitted.

References

[1] Y. Li, N. Jarrassé, and E. Burdet, "Versatile interaction control and haptic identification in humans and robots," in *Geometric and Numerical Foundations of Movements* (J.-P. Laumond, N. Mansard, and J.-B. Lasserre, eds.), vol. 117, pp. 187–206, Springer, 2017.

[2] O. Khatib, "A unified approach for motion and force control of robot manipulators: The operational space formulation," *IEEE Journal of Robotics and Automation*, vol. 3, no. 1, pp. 43–53, 1987.

[3] K. Kiguchi and T. Fukuda, "Position/force control of robot manipulators for geometrically unknown objects using fuzzy neural networks," *IEEE Transactions on Industrial Electronics*, vol. 47, pp. 641–649, Jun 2000.

[4] Z.-W. Luo, K. Ito, and M. Yamakita, "Estimation of environment models using vector field and its application to robot's contact tasks," in *Proceedings of IEEE International Conference on Neural Networks*, vol. 5, pp. 2546–2549, Nov 1995.

[5] N. Hogan, "Impedance control: An approach to manipulation," *Journal of Dynamic Systems, Measurement and Control, Transactions of the ASME*, vol. 107, no. 1, pp. 1–24, 1985.

[6] D. Braun, M. Howard, and S. Vijayakumar, "Optimal variable stiffness control: formulation and application to explosive movement tasks," *Autonomous Robots*, vol. 33, no. 3, pp. 237–53, 2012.

[7] A. Ajoudani, M. Gabiccini, N. Tsagarakis, and A. Bicchi, "Human-like impedance and minimum effort control for natural and efficient manipulation," in *IEEE International Conference on Robotics and Automation*, pp. 4499–505, 2013.

[8] M. Erden and A. Billard, "Robotic assistance by impedance compensation for hand movements while manual welding," *IEEE Transactions on Cybernetics*, vol. 46, pp. 2459–72, Nov 2016.

[9] E. Burdet, R. Osu, D. Franklin, T. Milner, and M. Kawato, "The central nervous system stabilizes unstable dynamics by learning optimal impedance," *Nature*, vol. 414, no. 6862, pp. 446–9, 2001.

[10] D. Franklin, R. Osu, E. Burdet, M. Kawato, and T. Milner, "Adaptation to stable and unstable dynamics achieved by combined impedance control and inverse dynamics model," *Journal of Neurophysiology*, vol. 90, no. 5, pp. 3270–82, 2003.

[11] D. Franklin, G. Liaw, T. Milner, R. Osu, E. Burdet, and M. Kawato, "Endpoint stiffness of the arm is directionally tuned to instability in the environment," *Journal of Neuroscience*, vol. 27, no. 29, pp. 7705–16, 2007.

[12] D. Franklin, E. Burdet, K. Tee, R. Osu, C. Chew, T. Milner, and M. Kawato, "CNS learns stable, accurate, and efficient movements using a simple algorithm," *Journal of Neuroscience*, vol. 28, no. 44, pp. 11165–73, 2008.

[13] K. Tee, D. Franklin, M. Kawato, T. Milner, and E. Burdet, "Concurrent adaptation of force and impedance in the redundant muscle system," *Biological Cybernetics*, vol. 102, no. 1, pp. 31–44, 2010.

[14] C. Yang, G. Ganesh, S. Haddadin, S. Parusel, A. Albu-Schaeffer, and E. Burdet, "Human-like adaptation of force and impedance in stable and unstable interactions," *IEEE Transactions on Robotics*, vol. 21, no. 5, pp. 918–30, 2011.

[15] V. Chib, J. Patton, K. Lynch, and F. Mussa-Ivaldi, "Haptic identification of surfaces as fields of force," *Journal of Neurophysiology*, vol. 95, no. 2, pp. 1068–77, 2005.

[16] M. Casadio, A. Pressman, and S. Mussa-Ivaldi, "Learning to push and learning to move: The adaptive control of contact forces," *Frontiers in Computational Neuroscience*, vol. 9, no. 118, 2015.

[17] A. Albu-Schäffer, C. Ott, and G. Hirzinger, "A unified passivity based control framework for position, torque and impedance control of flexible joint robots," *The International Journal of Robotics Research*, vol. 26, no. 1, pp. 23–39, 2007.

[18] A. Albu-Schäffer, O. Eiberger, M. Grebenstein, S. Haddadin, C. Ott, T. Wimbock, S. Wolf, and G. Hirzinger, "Soft robotics: From torque feedback controlled lightweight robots to intrinsically compliant systems," *IEEE Robotics and Automation Magazine*, vol. 15, no. 3, pp. 20–30, 2008.

[19] G. Ganesh, A. Albu-Schaeffer, M. Haruno, M. Kawato, and E. Burdet, "Biomimetic motor behavior for simultaneous adaptation of force, impedance and trajectory in interaction tasks," in *IEEE International Conference on Robotics and Automation*, pp. 2705–11, 2010.

[20] G. Ganesh, N. Jarrasse, S. Haddadin, A. Albu-Schaeffer, and E. Burdet, "A versatile biomimetic controller for contact tooling and haptic exploration," in *IEEE International Conference on Robotics and Automation*, pp. 3329–34, 2012.

[21] S. Arimoto, S. Kawamura, and F. Miyazaki, "Bettering operation of robots by learning," *Journal of Field Robotics*, vol. 1, no. 2, pp. 123–140, 1984.

[22] D. A. Bristow, M. Tharayil, and A. G. Alleyne, "A survey of iterative learning control," *IEEE Control Systems*, vol. 26, pp. 96–114, June 2006.

[23] Z. Bien and J.-X. Xu, *Iterative learning control: analysis, design, integration and applications*. Springer Science & Business Media, 2012.

[24] K. L. Moore, *Iterative learning control for deterministic systems*. Springer Science & Business Media, 2012.

[25] E. Burdet, A. Codourey, and L. Rey, "Experimental evaluation of nonlinear adaptive controllers," *IEEE Control Systems Magazine*, vol. 18, no. 2, pp. 39–47, 1998.

[26] K. Astrom and B. Wittenmark, *Adaptive control*. Reading: MA: Addison-Wesley, 1995.

[27] S. Jung, T. Hsia, and R. Bonitz, "Force tracking impedance control for robot manipulators with an unknown environment: theory, simulation, and experiment," *The International Journal of Robotics Research*, vol. 20, no. 9, pp. 765–74, 2001.

[28] R. Shadmehr and F. Mussa-Ivaldi, "Adaptive representation of dynamics during learning of a motor task," *The Journal of Neuroscience*, vol. 74, no. 5, pp. 3208–24, 1994.

[29] R. Osu, E. Burdet, D. Franklin, T. Milner, and M. Kawato, "Different mechanisms in adaptation to stable and unstable dynamics," *Journal of Neurophysiology*, vol. 90, no. 5, pp. 3255–69, 2003.

[30] K. Vaesen, "The cognitive bases of human tool use," *Behavioral and Brain Sciences*, vol. 35, no. 4, pp. 203–18, 2012.

[31] M. Haruno, G. Ganesh, E. Burdet, and M. Kawato, "Distinct neural correlates of reciprocal- and co-activation of muscles in dorsal and ventral premotor cortices," *Journal of Neurophysiology*, vol. 107, pp. 126–33, 2012.

[32] N. Jarrassé, T. Charalambous, and E. Burdet, "A framework to describe, analyze and generate interactive motor behaviors," *PLoS ONE*, vol. 7, no. 11, p. e49945, 2012.

[33] C. de Wit, B. Siciliano, and G. Bastin, *Theory of robot control*. Springer, 1996.